ACS APPLIED MATERIALS & INTERFACES
Research Article
www.acsami.org

Comparative Study on Electronic Structures of Sc and Ti Contacts with Monolayer and Multilayer MoS_2

Zhongjun Li,[†,‡] Xingxing Li,[†] and Jinlong Yang*[,†,§]

[†]Hefei National Laboratory for Physical Sciences at Microscale, University of Science and Technology of China, Hefei, Anhui 230026, China

[‡]School of Electronic Science and Applied Physics, Hefei University of Technology, Hefei, Anhui 230009, China

[§]Synergetic Innovation Center of Quantum Information and Quantum Physics, University of Science and Technology of China, Hefei, Anhui 230026, China

ABSTRACT: Understanding the nature of the contacts in devices based on MoS_2 with metal electrodes is vital to enhancing carrier injection efficiency. In this work, geometric and electronic structures of Sc and Ti contacts with MoS_2 have been comparatively studied by first-principles calculations. The analyses of geometric parameters, charge density distributions, and density of states for the Sc and Ti top contacts with monolayer MoS_2 ($mMoS_2$) indicate that the interface bonding results in the localization of 4d states of Mo atoms and the consequent metallization of $mMoS_2$. Therefore, the Sc and Ti top contacts with $mMoS_2$ are Ohmic, and electron injections via these contacts are efficient. Because of the formations of the metalized Sc−$mMoS_2$ and Ti−$mMoS_2$ complexes, in the Sc and Ti top contacts with multilayer MoS_2, Schottky interfaces may be formed in two contact regions. One is in the edge contacts of the Sc−$mMoS_2$ and Ti−$mMoS_2$ complexes with $mMoS_2$ in the channel region in which Schottky barrier heights of 0.11 and 0.39 eV are extracted, respectively. The other is in the top contacts of these two complexes with $mMoS_2$ under the contacts in which Schottky barrier heights of 0.15 and 0.34 eV are obtained, respectively. Moreover, as the layer number of MoS_2 increases in the top contacts, the Schottky barrier heights show decreasing trends. These trends can be understood on the basis of the changes of electron affinity of multilayer MoS_2. According to the present results, the device based on MoS_2 with Sc electrodes should have better electron injection efficiency and stronger back-gated manipulation of current than the one with Ti electrodes. Furthermore, the electron injection efficiency can be enhanced by using multilayer MoS_2. These predictions are generally consistent with recent experimental observations and provide a delicate understanding of the contacts in these devices.

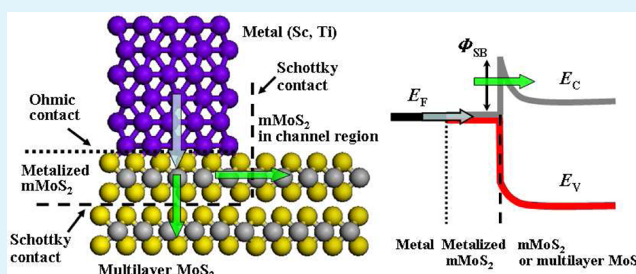

KEYWORDS: *MoS_2, Sc, metallization, Ohmic contact, Schottky contact*

1. INTRODUCTION

Molybdenum disulfide (MoS_2), especially monolayer MoS_2 ($mMoS_2$), shows many potential applications due to exotic electronic, optical, and mechanical properties.[1−11] A direct band gap of ∼1.8 eV enables $mMoS_2$ to be suitable not only for photocatalysis and photodetection but also for potential applications in field effect transistors (FET). In particular, the ultrathin thickness allows $mMoS_2$ to exhibit small short channel effects and excellent electrostatic modulation as contacts with dielectrics in FET.[7−9] Hence, in recent years, many electronic, spintronic, optoelectronic, and photochemical devices have been fabricated based on MoS_2.[7−19] In these devices, excellent performances, such as high current on/off ratio,[10] strong current spin-polarization,[12,13] and high photoresponsivity,[16] have been achieved. However, further performance improvements for these devices have been limited by relatively low carrier mobility. For this limitation to be overcome, it is vital that the carrier injection efficiency from metal electrodes to MoS_2 be enhanced.[20,21] Therefore, at the present stage, great efforts have been made to improve metal contacts with MoS_2.[22−32]

It is generally accepted in conventional Schottky theory that metals with low or high work functions can be employed to obtain *n*-type or *p*-type Schottky contacts, respectively, with MoS_2, and Ohmic contacts may be achieved by choosing metal materials with suitable work functions to MoS_2. However, it is difficult to achieve stable and controllable Ohmic contact in experiments due to the influences of some unknown factors. For example, Ohmic and Schottky contacts were claimed to be formed in the Au−MoS_2 junction and in the $mMoS_2$ transistor with Au electrodes by different groups, respectively.[10,25] In a back-gated FET based on bilayer MoS_2 with Ti electrodes, an *n*-type Ohmic contact was observed at room temperature whereas a Schottky barrier was found at lower temperatures.[26] A recent experimental study showed that the FET based on MoS_2 flakes

Received: March 31, 2015
Accepted: May 27, 2015
Published: May 27, 2015

ACS Publications © 2015 American Chemical Society

DOI: 10.1021/acsami.5b02782
ACS Appl. Mater. Interfaces 2015, 7, 12981−12987

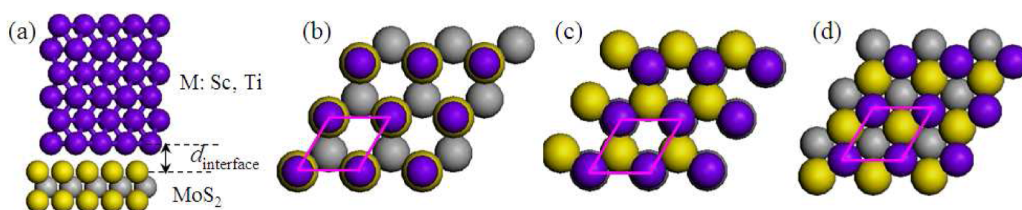

Figure 1. (a) Schematics of top contacts; top views of (b) TS configuration, (c) TM configuration, and (d) TH configuration for Sc and Ti top contacts with $mMoS_2$. For clarity, only the Sc and Ti atoms in the first layer were presented. Blue, yellow, and gray balls represent metal atoms of Sc or Ti, S atoms, and Mo atoms, respectively.

with Sc electrodes has lower *n*-type Schottky barriers than those with Ti, Ni, and Pt electrodes.[27] Because MoS_2 flakes, not $mMoS_2$, were employed in the experiments described above, the carrier injection processes are quite complicated.

For the factors that influence contact performances to be explored, several theoretical studies on metal contacts with $mMoS_2$ have been carried out. According to the calculated results, Popov et al. found that the nature of the Au and Ti contacts with $mMoS_2$ is more general contact tunnel barrier rather than conventional Schottky barrier and proposed Ti as a more suitable alternative electrode material than widely used Au.[28] Gong et al. studied Al, Ag, Au, Pd, Ir, and Pt contacts with $mMoS_2$ and revealed an abnormal Fermi level pinning mechanism at the interfaces.[29] In a recent theoretical study on In, Au, Pd, and Ti contacts with $mMoS_2$ and $mWSe_2$, Kang et al. observed metallization of $mMoS_2$ and proposed Ti and Mo as favorable electrode materials.[30] Although these theoretical studies have promoted the understanding of the experimental results, the factors involved in the formation of a metal-MoS_2 interface, such as the metallization and Fermi level pinning, are not yet well understood. More noteworthy in these theoretical studies is that only metals with work functions larger than the electron affinity of $mMoS_2$ were employed, among which Ti was proposed to be the most suitable.[28−31] However, the experimental study showed that Sc with a work function lower than MoS_2 forms better contacts with MoS_2.[27] Therefore, it is necessary to perform a comparative theoretical study to present a more detailed understanding of Sc and Ti contacts with MoS_2 and further reveal which factors determine contact performances at the atomic scale. As far as we know, such a study, especially one on Sc contact with $mMoS_2$, has not been reported to date.

In the present work, we report a comparative study on Sc and Ti contacts with $mMoS_2$ and multilayer MoS_2 by first-principles calculations based on the density functional theory method. First, stable configurations for the Sc and Ti top contacts with $mMoS_2$ are determined. Second, on the basis of the analyses of geometric parameters, density of states (DOS), charge density distributions, and band structures, the nature of the Sc and Ti contacts with $mMoS_2$ and multilayer MoS_2 is revealed. Finally, on the basis of the present theoretical results, a delicate understanding of recent experimental results is presented.

2. COMPUTATIONAL METHOD

The present first-principles calculations were carried out based on density functional theory (DFT) using the Vienna ab initio simulation package (VASP) with projector-augmented wave (PAW) pseudopotentials.[33,34] Local density approximation (LDA) was employed to describe the exchange and correlation interactions with the partial core correction included,[35] which is suitable for describing the metal−MoS_2 contact.[23,28,29] The computational model is presented in Figure 1a. The $mMoS_2$ was placed on the (0001) surfaces of Sc and Ti, which were found to be most stable in the previous experiments. In the calculations, the metal slabs were extended to the sixth and tenth atomic layer. The calculated results indicate that the slabs with six atomic layers are enough to simulate metal surfaces. Therefore, only the calculated results based on the slabs with six atomic layers are presented in the present work. A vacuum region more than 25 Å normal to the surface was added to remove the coupling between adjacent slabs. Geometry structures were relaxed until the force on each atom is less than 0.01 eV/Å, and the convergence criteria is 10^{-4} eV for energy. During ionic relaxation, the shape and size of the super cell were fixed, and all other atoms, including Mo and S atoms, were fully relaxed except for the metal atoms in the three bottom layers, which were fixed at their respective bulk positions. The Monkhorst−Pack k-point sampling in Brillouin zone was Γ-centered with 8 × 8 × 1 and 16 × 16 × 1 meshes in ionic and electronic optimization, respectively. A kinetic-energy cutoff of 400 eV was chosen for the plane wave basis set.

For the configuration stability to be evaluated, the binding energy between the metals of Sc and Ti and $mMoS_2$ was calculated by the formula

$$E_b = E_{\text{metal}-\text{mMoS}_2} - (E_{\text{metal}} + E_{\text{mMoS}_2})$$

where E_{metal}, E_{mMoS_2}, and $E_{\text{metal}-\text{mMoS}_2}$ denote energies of isolated metal slabs of Sc and Ti, isolated $mMoS_2$ monolayer, and the composite of the metal slab and $mMoS_2$, respectively. The charge difference analysis between complexes, metals, and isolated $mMoS_2$ was performed using the formula

$$\Delta\rho = \rho_{\text{metal}-\text{mMoS}_2} - (\rho_{\text{metal}} + \rho_{\text{mMoS}_2})$$

where the charge densities of ρ_{metal}, ρ_{mMoS_2}, and $\rho_{\text{metal}-\text{mMoS}_2}$ are averaged in the planes parallel to the interface. By charge difference analysis, the charge redistribution along the *Z*-direction normal to the interface was derived.

3. RESULTS AND DISCUSSION

3.1. Geometric Structures. The interaction in the Sc and Ti top contacts with $mMoS_2$ is sensitive to stacking configurations. Figure 1a presents the schematics for the metal top contact with $mMoS_2$. Three types of stacking configurations were considered for each contact, respectively, as shown in Figure 1b−d. The optimized lattice constant of $mMoS_2$ is 3.12 Å. For comparison, in Sc and Ti top contacts with $mMoS_2$, the lattice constant of $mMoS_2$ was kept constant, and the (0001) surfaces of Sc and Ti were extended and strained to match the lattice constant of $mMoS_2$ in all calculations as was done by Gong et al.[29] In the TS

Table 1. Equilibrium Interface Distance (d), Bond Length (d), and Binding Energy per Unit Cell (E_b) for the Three Configurations of Sc and Ti top contacts with $mMoS_2$[a]

metal−$mMoS_2$	configuration	$d_{interface}$	$d_{metal-S1}$	d_{Mo-S1}	d_{Mo-S2}	E_b
Sc(0001)−MoS_2	TS	2.636	2.636	2.419	2.391	−0.87
	TM	1.815	2.583	2.466	2.385	−1.63
	TH	2.000	2.734	2.480	2.384	−1.08
Ti(0001)−MoS_2	TS	2.445	2.445	2.406	2.380	−0.92
	TM	1.650	2.442	2.495	2.386	−2.14
	TH	1.605	2.411	2.482	2.369	−2.09

[a]Equilibrium distance and bond length are in Å; binding energy per unit cell is in eV. The $d_{interface}$ is the equilibrium interface distance between the topmost S layer and the first metal layer, and S1 and S2 denote the topmost and the bottom most S atoms, respectively.

configuration, the Sc and Ti atoms in the first layer are directly above the topmost S atoms. In the TM configuration, the Sc and Ti atoms are on top of Mo atoms. In the TH configuration, the Sc and Ti atoms are situated on the hollow site of the hexagons of $mMoS_2$.

For these three types of stacking configurations, the optimized structural parameters are listed in Table 1 together with the binding energies per unit cell. The binding energies of the Sc and Ti top contacts with $mMoS_2$ clearly depend on the adsorption sites. For each metal top contact with $mMoS_2$, the TM and TH configurations have smaller interface distances than the TS configuration. Moreover, in the TM configuration, the Sc and Ti atoms in the first layer and the Mo atoms are located at two sides of the topmost S layer. This symmetric arrangement facilitates bonding between the topmost S atoms and the Sc and Ti atoms. Thus, the TM configuration has the largest binding energy among these three configurations. On the other hand, for each stacking configuration, the Ti top contact with $mMoS_2$ has a smaller interface distance and larger binding energy than the Sc top contact, indicating that the bonding between S and Ti atoms is stronger than that between S and Sc atoms. Therefore, the Sc and Ti top contacts to $mMoS_2$ with the TM configuration, denoted as Sc−$mMoS_2$ and Ti−$mMoS_2$ complexes, are emphatically studied in the following sections.

As listed in Table 1, there are obvious differences in the geometric parameters between the Sc−$mMoS_2$ and Ti−$mMoS_2$ complexes. The interface distances are 1.815 and 1.650 Å, respectively, for these two complexes. Such short interlayer distances facilitate substantial bonding between the topmost S atoms and the Sc and Ti atoms, as demonstrated by the S1−Sc and S1−Ti bond lengths of 2.583 and 2.442 Å. These substantial bonds may weaken the interaction between the topmost S atoms and the Mo atoms. Therefore, the bonds between the topmost S and Mo atoms show longer lengths than those between the bottom most S and Mo atoms. Besides, for the geometric parameters, the electronic structures of the Sc−$mMoS_2$ and Ti−$mMoS_2$ complexes also show obvious differences, as discussed in subsequent sections.

3.2. Density of States and Metallization of MoS_2.

Total DOS and the projected DOS on $mMoS_2$, Sc, and Ti atoms are given in Figure 2 for the Sc−$mMoS_2$ and Ti−$mMoS_2$ complexes. For clarity, the projected DOS on $mMoS_2$ were multiplied by a factor of 6.0 according to the metal atom number ratios in the super cell. Total DOS show that these two complexes are metallic. Near the Fermi level, the intensity of total DOS in the former complex is larger than that in the latter. For these two complexes, the projected DOS on $mMoS_2$ show that, compared with isolated $mMoS_2$, some electron states occur in the band gap and the gap clearly decreases. Also shown

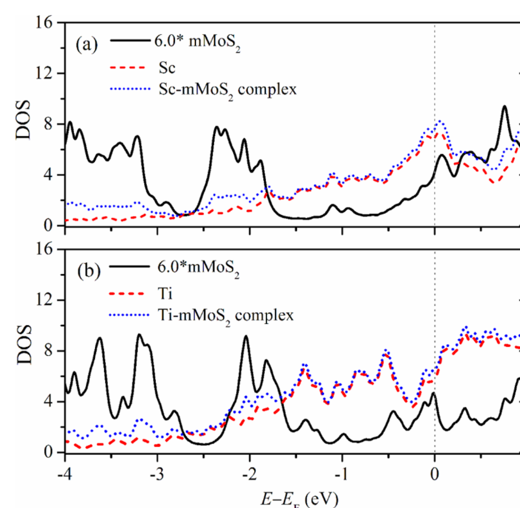

Figure 2. Total DOS and projected DOS on Sc, Ti, and $mMoS_2$ for (a) Sc−$mMoS_2$ and (b) Ti−$mMoS_2$ complexes.

is that these electron states in the band gap of $mMoS_2$ in the Sc−$mMoS_2$ complex are more continuous than those in the Ti−$mMoS_2$ complex. Because of the appearance of these gap states, the Fermi level shifts above the bottom of the conduction band and essentially overlaps with the conduction bands of $mMoS_2$. Therefore, the $mMoS_2$ in the Sc−$mMoS_2$ and Ti−$mMoS_2$ complexes are metallized.

3.3. Charge Transfer and Interface Bonding.

The metallization of $mMoS_2$ in the Sc−$mMoS_2$ and Ti−$mMoS_2$ complexes can be analyzed by interface charge distribution and interface bonding. As shown in Figure 3, the Sc−$mMoS_2$ interface has approximately equivalent charge density to the Sc−Sc interlayers whereas the Ti−$mMoS_2$ interface exhibits larger charge density than the Ti−Ti interlayers. In the S1−Mo and S2−Mo interlayers of the Sc−$mMoS_2$ complex, symmetrical charge distributions are observed, and the Mo atoms have more charge density than the S atoms. In the Ti−$mMoS_2$ complex, the S atoms possess more charge density than the Mo atoms, and the charge density near the Mo atoms show a clearly nonsymmetrical distribution (i.e., the S1−Mo interlayer has a smaller charge density than that of S2−Mo). These nonsymmetrical charge distributions are consistent with the unequal lengths of the S1−Mo and S2−Mo bonds, as listed in Table 1. The nonsymmetrical characteristics in the charge distributions and bond lengths should be attributed to the strong interface bonding between the S1 and Ti1 atoms.

The interface bonding in the Sc−$mMoS_2$ and Ti−$mMoS_2$ complexes can be further investigated by charge difference analysis. The appearances of charge depletion and accumulation

DOI: 10.1021/acsami.5b02782
ACS Appl. Mater. Interfaces 2015, 7, 12981−12987

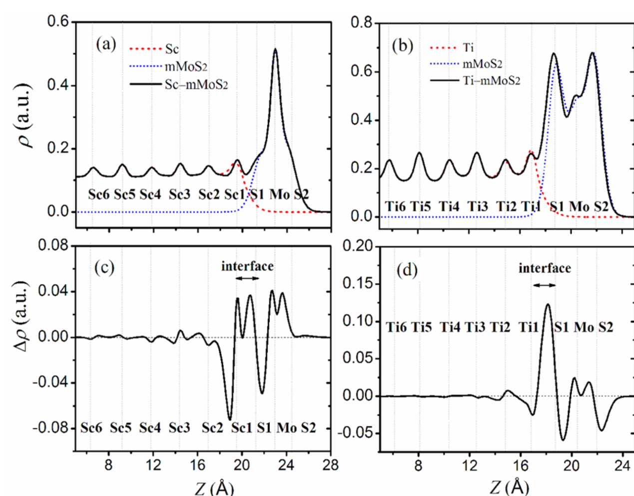

Figure 3. Plane-averaged charge density along the Z-direction normal to the interface for (a) Sc slab, $mMoS_2$, and Sc−$mMoS_2$ complex, and (b) Ti slab, $mMoS_2$, and Ti−$mMoS_2$ complex, and the corresponding charge difference for the (c) Sc−$mMoS_2$ complex and (d) Ti−$mMoS_2$ complex.

in different regions denote the charge transfer among them. As shown in Figure 3c, when the interface is formed in the Sc−$mMoS_2$ complex, on one hand, charge transfers occur from the Sc1−Sc2 and S1−Mo interlayers to the Sc−$mMoS_2$ interface, and two charge accumulation regions occur in the interface. These charge transfers make the Sc1−Sc2 and S1−Mo bonds weaker and enable the Sc1−S1 bonds to be substantially formed. On the other hand, charge transfer also occurs from the S1−Mo interlayers to Mo atoms, indicating the localization of the charge toward Mo atoms. Compared with the Sc−$mMoS_2$ complex, similar charge transfers are observed in the Ti−$mMoS_2$ complex except for the slight difference that only one charge accumulation region appears in the Ti−$mMoS_2$ interface, as shown in Figure 3d. The charge accumulations in the Sc−$mMoS_2$ and Ti−$mMoS_2$ interfaces denote the substantial bonding between the topmost S atoms and the Sc and Ti atoms.

Here, the charge density distributions in the Sc and Ti top contacts with $mMoS_2$ are also compared with those in the widely used Au contact. As observed by Gong et al. in the Au−$mMoS_2$ complex, one charge accumulation region and two charge depletion regions appear simultaneously in the Au−MoS_2 interface, and charge density shows almost no change in other regions.[29] This charge redistribution is attributed to the surface charge repulsion effect, demonstrating no chemical bonding in the Au−MoS_2 interface.[29]

Kang et al. suggested that a metal top contact with a semiconductor can be clarified into three types of interfaces: type 1, very weak adhesion; type 2, medium adhesion; and type 3, strong adhesion.[30] In type 1, there is no chemical bonding between the metal and semiconductor due to a large interface distance. In type 2, a medium interface distance results in weak chemical bonding. In type 3, a small interface distance leads to strong chemical bonding and substantial metallization of the semiconductor, resulting in an Ohmic interface. In light of the interface distances and charge distribution, the Sc and Ti top contacts with $mMoS_2$ should have strong adhesion, and the nature of the contacts is Ohmic, whereas the Au top contact with $mMoS_2$ has at most medium adhesion.

3.4. Partial Density of States and Nature of the Metallization.

As discussed above, the interface bonding and the consequent metallization are vital to achieving Ohmic contact. The metallization of $mMoS_2$ in the Sc−$mMoS_2$ and Ti−$mMoS_2$ complexes can be revealed more details by the evolutions of PDOS with different interface distances. Figure 4 presents the evolutions of PDOS with three different interface distances for the Sc−$mMoS_2$ complex.

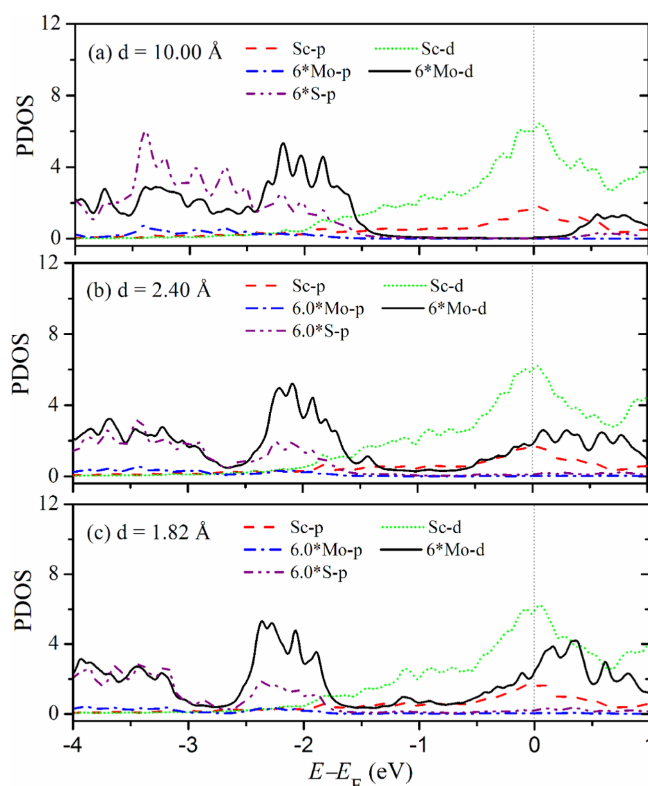

Figure 4. Evolutions of PDOS for the Sc top contact with $mMoS_2$ with three different interface distances: (a) d = 10.00, (b) d = 2.40, and (c) d = 1.82 Å.

It can be seen from Figure 4 that the bottom of the conduction band and the top of the valence band of $mMoS_2$ mainly consist of the 4d states of Mo atoms coupled with small amounts of 2p states of S atoms. The 3d states of Sc atoms dominate the components of the conduction band together with the 3p states. As shown in Figure 4a, when the interface distance is large enough, the interaction between $mMoS_2$ and Sc surfaces is negligible, and the PDOS of 4d states of Mo atoms exhibit a similar band gap to that of isolated $mMoS_2$. When the interlayer distances decrease to that of the equilibrium one, the conduction band contributed from 4d states of Mo atoms shifts down significantly, and the corresponding valence band shifts slightly, as shown in Figure 4b,c. These shifts lead to an obvious decrease of the band gap and essential crossing of 4d states of Mo atoms with the Fermi level, and the Sc−$mMoS_2$ interface becomes metallic. Similar cases are observed for the Ti−$mMoS_2$ complex.

On the basis of the charge transfer and PDOS analyses, the metallization of the Sc−$mMoS_2$ and Ti−$mMoS_2$ interfaces can be understood according to atomic orbital energy level correlation. As mentioned above, the conduction and valence bands of $mMoS_2$ mainly consist of the 4d states of Mo atoms

DOI: 10.1021/acsami.5b02782
ACS Appl. Mater. Interfaces 2015, 7, 12981−12987

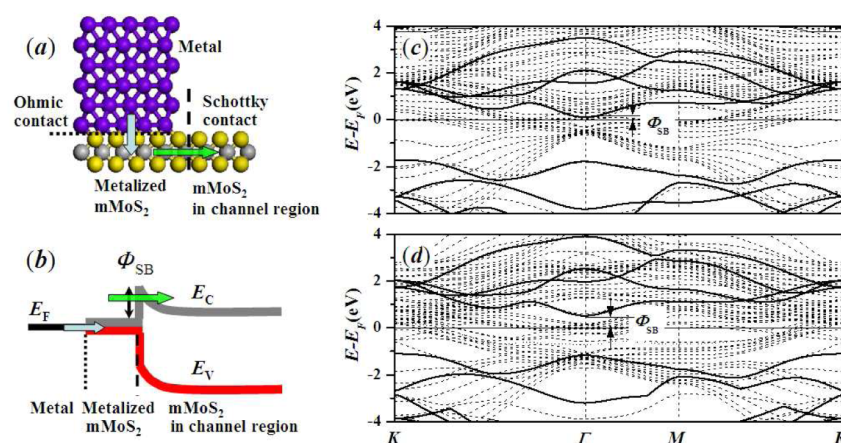

Figure 5. (a) Interface schematics, (b) band diagrams, and (c, d) band structures for the Sc-mMoS$_2$ and Ti-mMoS$_2$ complexes. The band structures of isolated mMoS$_2$ without contact are also superimposed in the figure for reference.

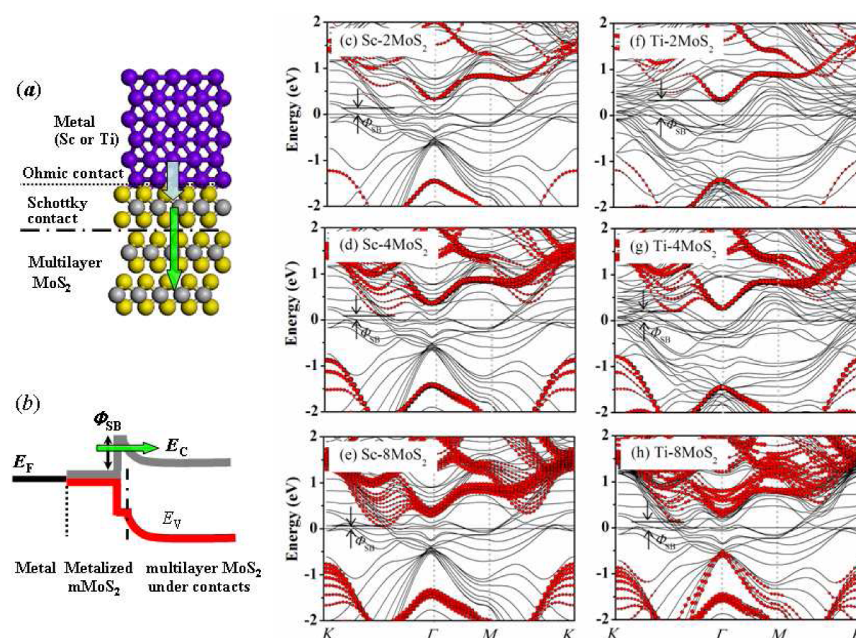

Figure 6. (a) Interface schematics, (b) band diagrams, and band structures for the (c−e) Sc and (f−h) Ti top contacts with 2-, 4-, and 8-layer MoS$_2$, respectively. The red dots represent the projected band structures on the underlying MoS$_2$ with 1, 3, and 7 layers, and the dot size denotes the weight.

coupled with small amounts of 2p states of S atoms. The 4d states of Mo atoms and the 2p states of S atoms split into bonding and antibonding states. In a periodic potential field, these bonding and antibonding states form the valence and conduction bands of isolated mMoS$_2$. When mMoS$_2$ contacts the Sc and Ti surfaces, the bonding between the topmost S atoms and the Sc and Ti atoms weaken the bonding between the topmost S and Mo atoms and consequently result in the localization of 4d states of Mo atoms and 2p states of S atoms. Therefore, the nature of the metallization of mMoS$_2$ in the Sc−mMoS$_2$ and Ti−mMoS$_2$ complexes is the localization of 4d states of Mo atoms toward Fermi levels.

3.5. Band Alignments and Schottky Contacts. Because of the metallization of the Sc−mMoS$_2$ and Ti−mMoS$_2$ complexes, Schottky barriers may be formed in two contact regions: one is the edge contacts of these two complexes with mMoS$_2$ in the channel region; the other is the top contacts of these two complexes with multilayer MoS$_2$, as shown in Figures 5a and 6a. The corresponding band diagrams for these two contacts are presented in Figures 5b and 6b.

Pancels c and d of Figure 5 present the band structures of the Sc−mMoS$_2$ and Ti−mMoS$_2$ complexes, respectively. To extract the Schottky barrier height in the edge contacts of these two complexes with mMoS$_2$ in the channel region, the band structure of isolated mMoS$_2$ is also superimposed in each figure. As revealed by the band alignments, both Sc−mMoS$_2$ and Ti−mMoS$_2$ complexes form *n*-type Schottky contacts with mMoS$_2$ in the channel region. The Schottky barrier height in the former edge contact is ∼0.11 eV, lower than 0.39 eV in the latter. The obtained Schottky barrier height in the Ti contact with mMoS$_2$ is in agreement with the previous theoretical prediction of 0.33 eV.[30]

For the top contacts, to extract the Schottky barrier heights and evaluate the corresponding influences of the layer numbers of MoS$_2$, the band structures of Sc and Ti top contacts with 2-, 4-, and 8-layer MoS$_2$ are given in Figure 6c−e and 6f−h,

DOI: 10.1021/acsami.5b02782
ACS Appl. Mater. Interfaces 2015, 7, 12981−12987

respectively. The projected band structures on 1-, 3-, and 7-layer MoS_2 are marked by red dots, and the weight is denoted by the dot size. It can be seen from Figure 6 that the first MoS_2 layer is metallized, the underlying MoS_2 with 1, 3, and 7 layers are preserved to be semiconducting. Therefore, the *n*-type Schottky interfaces are substantially formed in the top contacts of Sc-mMoS_2 and Ti-mMoS_2 complexes with the underlying MoS_2. The obtained Schottky barrier heights are approximately 0.15 and 0.34 eV in the top contacts of Sc-mMoS_2 and Ti-mMoS_2 complexes with 1-layer MoS_2, respectively. These values are almost equivalent to Schottky barrier heights of 0.11 and 0.39 eV obtained in the edge contacts of Sc-mMoS_2 and Ti-mMoS_2 complexes, respectively, with mMoS_2 in the channel region.

As the underlying MoS_2 increases from 1 to 3 to 7 layers, the Schottky barrier heights decrease from 0.15 to 0.11 to 0.05 eV for the top contact of the Sc-mMoS_2 complex with MoS_2, and from 0.34 to 0.25 to 0.13 eV for that of the Ti-mMoS_2 complex, as shown in Figure 6c−e and 6f−h, respectively. The variation trends can be qualitatively understood by the changes of electron affinity of multilayer MoS_2. The calculated electron affinity increases from 4.49 to 4.59 to 4.98 eV when the MoS_2 increase from 1 to 3 to 7 layers, respectively. The increase of electron affinity should lead to the decrease of Schottky barrier heights in the top contacts of Sc−MoS_2 and Ti−mMoS_2 complexes with multilayer MoS_2. According to the present calculations, regardless of the edge and top contacts, the device based on mMoS_2 and multilayer MoS_2 with Sc electrodes should have better electron injection efficiency and stronger back-gated manipulations on current than the one with Ti electrodes due to a lower Schottky barrier height in the former device. These predictions are generally consistent with the experimental observations by Das et al.[27] It is noted here that the calculated Schottky barrier heights in the top contacts of Sc and Ti with MoS_2 are larger than the experimental values of 0.03 and 0.05 eV, respectively.[27]

These differences may come from two aspects in light of the theoretical and experimental details. One is from the geometric models employed in the present calculations. We note that the experimental values were measured using MoS_2 flakes with thicknesses of ∼100 Å. The maximum thickness of multilayer MoS_2 is clearly smaller than 100 Å in the present work. Also, we note a trend observed in the experiments that the extracted effective field effect mobility obviously increases and the corresponding Schottky barrier height decreases as the thickness of the MoS_2 layer increases from 20 to 100 Å.[26] This decreasing trend is in accordance with the present calculated results in which the Schottky barrier height decreases as MoS_2 increases from 2 to 4 to 8 layers. The other is from the theoretical method. The LDA employed in the present work does not give accurate predictions of band gaps for some semiconductor materials. Accurate descriptions of electronic structures for semiconductor materials need to employ higher theoretical methods to fully consider many-body effects among electrons. However, LDA has significant computational advantages over other ab initio methods. Moreover, LDA is widely used to describe the exchange and correlation interactions with the partial core correction included in the metal−MoS_2 contacts because the strong Coulomb screening by metal slabs with an infinite dielectric constant may minimize many-body effects in MoS_2.[23,28,29] Considering these aspects, we believe that the present calculations can give a qualitative understanding of the experimental results even though there are some differences between the theoretical and experimental results.

4. CONCLUSIONS

In conclusion, a comparative study on the electronic structures of Sc and Ti contacts with mMoS_2 have been reported, and Ohmic and Schottky interfaces are observed in each metal contact with MoS_2. Ohmic interfaces are formed in the Sc and Ti top contacts with mMoS_2 due to interface bonding and the consequent metallization, and the contact resistance effects are almost eliminated. Therefore, electron injection via these top contacts should be highly efficient. Because of the metallization of mMoS_2 in the Sc−mMoS_2 and Ti−mMoS_2 complexes, Schottky interfaces are formed both in the edge contacts of these two metallized complexes with mMoS_2 in the channel region and in the top contacts of these two complexes with multilayer MoS_2 under the contacs. The Sc contact with MoS_2 has lower Schottky barriers than the Ti contacts regardless of the edge or top contacts. Moreover, in the top contacts of Sc and Ti with multilayer MoS_2, the Schottky barrier heights show decreasing trends as the layer numbers of MoS_2 increase. According to the present calculated results, the device based on mMoS_2 and multilayer MoS_2 with Sc electrodes should have a better electron injection efficiency and stronger back-gated manipulation on current than the one with Ti electrodes. These predictions are generally consistent with the recent experimental observations and provide a more delicate understanding of the contacts in these devices.

■ AUTHOR INFORMATION

Corresponding Author

*Phone: 86-551-63606408. E-mail: jlyang@ustc.edu.cn.

Notes

The authors declare no competing financial interest.

■ ACKNOWLEDGMENTS

This work is partially supported by the National Key Basic Research Program (2011CB921404), NSFC (21421063, 91021004, 21233007), Chinese Academy of Sciences (CAS) (XDB01020300), CPSF (2012M521235), Fundamental Research Funds for the Central Universities (JZ2015HGXJ0184), and the USTCSCC, SCCAS, Tianjin, and Shanghai Supercomputer Centers.

■ REFERENCES

(1) Mak, K. F.; Lee, C.; Hone, J.; Shan, J.; Heinz, T. F. Atomically Thin MoS_2: a New Direct-Gap Semiconductor. *Phys. Rev. Lett.* **2010**, *105*, 136805/1−4.
(2) Salmani, J. M.; Tan, Y.; Klimeck, G. Single Layer MoS_2 Band Structure and Transport. *Int. Semicond. Device. Res. Symp., 5th* **2011**, *517*, 1−2.
(3) Amani, M.; Chin, M. L.; Birdwell, A. G.; O'Regan, T. P.; Najmaei, S.; Liu, Z.; Ajayan, P. M.; Lou, J.; Dubey, M. Electrical Performance of Monolayer MoS_2 Field-Effect Transistors Prepared by Chemical Vapor Deposition. *Appl. Phys. Lett.* **2013**, *102*, 193107/1−4.
(4) Zeng, H. L.; Dai, J. F.; Yao, W.; Xiao, D.; Cui, X. D. Valley Polarization in MoS_2 Monolayers by Optical Pumping. *Nat. Nanotechnol.* **2012**, *7*, 490−493.
(5) Splendiani, A.; Sun, L.; Zhang, Y. B.; Li, T. S.; Kim, J.; Chim, C. Y.; Galli, G.; Wang, F. Emerging Photoluminescence in Monolayer MoS_2. *Nano Lett.* **2010**, *10*, 1271−1275.
(6) Bertolazzi, S.; Brivio, J.; Kis, A. Stretching and Breaking of Ultrathin MoS_2. *ACS Nano* **2011**, *5*, 9703−9709.

DOI: 10.1021/acsami.5b02782
ACS Appl. Mater. Interfaces 2015, 7, 12981−12987

(7) Liu, H.; Neal, A. T.; Ye, P. D. Channel Length Scaling of MoS_2 MOSFETs. *ACS Nano* **2012**, *6*, 8563−8569.
(8) Ghatak, S.; Ghosh, A. Observation of Trap-Assisted Space Charge Limited Conductivity in Short Channel MoS_2 Transistor. *Appl. Phys. Lett.* **2013**, *103*, 122103/1−5.
(9) Liu, H.; Ye, P. D. MoS_2 Dual-Gate MOSFET With Atomic-Layer-Deposited Al_2O_3 as Top-Gate Dielectric. *IEEE Electron Device Lett.* **2012**, *33*, 546−548.
(10) Radisavljevic, B.; Radenovic, A.; Brivio, J.; Giacometti, V.; Kis, A. Single-layer MoS_2 transistors. *Nat. Nanotechnol.* **2011**, *6*, 147−150.
(11) Lu, N.; Guo, H. Y.; Wang, L.; Wu, X. J.; Zeng, X. C. Van der Waals Trilayers and Superlattices: Modification of Electronic Structures of MoS_2 by Intercalation. *Nanoscale* **2014**, *6*, 4566−4571.
(12) Xiao, D.; Liu, G. B.; Feng, W. X.; Xu, X. D.; Yao, W. Coupled Spin and Valley Physics in Monolayers of MoS_2 and Other Group-VI Dichalcogenides. *Phys. Rev. Lett.* **2012**, *108*, 196802/1−5.
(13) Myoung, N.; Seo, K.; Lee, S. J.; Ihm, G. Large Current Modulation and Spin-Dependent Tunneling of Vertical Graphene/MoS_2 Heterostructures. *ACS Nano* **2013**, *7*, 7021−7027.
(14) Lopez-Sanchez, O.; Lembke, D.; Kayci, M.; Radenovic, A.; Kis, A. Ultrasensitive Photodetectors Based on Monolayer MoS_2. *Nat. Nanotechnol.* **2013**, *8*, 497−501.
(15) Zhang, W. J.; Huang, J. K.; Chen, C. H.; Chang, Y. H.; Cheng, Y. J.; Li, L. J. High-Gain Phototransistors Based on a CVD MoS_2 Monolayer. *Adv. Mater.* **2013**, *25*, 3456−3461.
(16) Choi, W.; Cho, M. Y.; Konar, A.; Lee, J. H.; Cha, G. B.; Hong, S. C.; Kim, S.; Kim, J.; Jena, D.; Joo, J.; Kim, S. High-Detectivity Multilayer MoS_2 Phototransistors With Spectral Response From Ultraviolet to Infrared. *Adv. Mater.* **2012**, *24*, 5832−5836.
(17) Li, H.; Yin, Z. Y.; He, Q. Y.; Li, H.; Huang, X.; Lu, G.; Fam, D. W. H.; Tok, A. I. Y.; Zhang, Q.; Zhang, H. Fabrication of Single- and Multilayer MoS_2 Film-Based Field-Effect Transistors for Sensing NO at Room Temperature. *Small* **2012**, *8*, 63−67.
(18) Jaramillo, T. F.; Jorgensen, K. P.; Bonde, J.; Nielsen, J. H.; Horch, S.; Chorkendorff, I. Identification of Active Edge Sites for Electrochemical H_2 Evolution From MoS_2 Nanocatalysts. *Science* **2007**, *317*, 100−102.
(19) Xiang, Q. J.; Yu, J. G.; Jaroniec, M. Synergetic Effect of MoS_2 and Graphene as Cocatalysts for Enhanced Photocatalytic H_2 Production Activity of TiO_2 Nanoparticles. *J. Am. Chem. Soc.* **2012**, *134*, 6575−6578.
(20) Yoon, Y.; Ganapathi, K.; Salahuddin, S. How Good Can Monolayer MoS_2 Transistors Be? *Nano Lett.* **2011**, *11*, 3768−3773.
(21) Jena, D.; Konar, A. Enhancement of Carrier Mobility in Semiconductor Nanostructures by Dielectric Engineering. *Phys. Rev. Lett.* **2007**, *98*, 136805/1−5.
(22) Liu, H.; Si, M. W.; Deng, Y. X.; Neal, A. T.; Du, Y. C.; Najmaei, S.; Ajayan, P. M.; Lou, J.; Ye, P. D. Switching Mechanism in Single-Layer Molybdenum Disulfide Transistors: An Insight into Current Flow across Schottky Barriers. *ACS Nano* **2014**, *8*, 1031−1038.
(23) Chen, W.; Santos, E. J. G.; Zhu, W. G.; Kaxiras, E.; Zhang, Z. Y. Tuning the Electronic and Chemical Properties of Monolayer MoS_2 Adsorbed on Transition Metal Substrates. *Nano Lett.* **2013**, *13*, 509−514.
(24) Neal, A. T.; Liu, H.; Gu, J. J.; Ye, P. D. Metal Contacts with MoS_2: A Two-dimensional Semiconductor. *Device Research Conference* **2012**, 65−66.
(25) Fontana, M.; Deppe, T.; Boyd, A. K.; Rinzan, M.; Liu, A. Y.; Paranjape, M.; Barbara, P. Electron-Hole Tansport and Photovoltaic Effect in Gated MoS_2 Schottky Junctions. *Sci. Rep.* **2013**, *3*, 1634/1−5.
(26) Qiu, H.; Pan, L. J.; Yao, Z. N.; Li, J. J.; Shi, Y.; Wang, X. R. Electrical Characterization of Back-Gated Bi-Layer MoS_2 Field-Effect Transistors and the Effect of Ambient on their Performances. *Appl. Phys. Lett.* **2012**, *100*, 123104/1−4.
(27) Das, S.; Chen, H. Y.; Penumatcha, A. V.; Appenzeller, J. High Performance Multilayer MoS_2 Transistors with Scandium Contacts. *Nano Lett.* **2013**, *13*, 100−105.
(28) Popov, I.; Seifert, G.; Tomanek, D. Designing Electrical Contacts to MoS_2 Monolayers: A Computational Study. *Phys. Rev. Lett.* **2012**, *108*, 156802/1−5.
(29) Gong, C.; Colombo, L.; Wallace, R. M.; Cho, K. The Unusual Mechanism of Partial Fermi Level Pinning at Metal-MoS_2 Interfaces. *Nano Lett.* **2014**, *14*, 1714−1720.
(30) Kang, J. H.; Liu, W.; Sarkar, D.; Jena, D.; Banerjee, K. Computational Study of Metal Contacts to Monolayer Transition-Metal Dichalcogenide Semiconductors. *Phys. Rev. X* **2014**, *4*, 031005/1−14.
(31) Kang, J. H.; Liu, W.; Banerjee, K. High-performance MoS_2 Transistors with Low-resistance Molybdenum Contacts. *Appl. Phys. Lett.* **2014**, *104*, 093106/1−6.
(32) Pradhan, N. R.; Rhodes, D.; Zhang, Q.; Talapatra, S.; Terrones, M.; Ajayan, P. M.; Balicas, L. Intrinsic Carrier Mobility of Multi-layered MoS_2 Field-effect Transistors on SiO_2. *Appl. Phys. Lett.* **2013**, *102*, 123105/1−5.
(33) Kresse, G.; Furthmuller, J. Efficiency of Ab-Initio Total Energy Calculations for Metals and Semiconductors Using a Plane-wave Basis Set. *Comput. Mater. Sci.* **1996**, *6*, 15−50.
(34) Blochl, P. E. Projector Augmented-Wave Method. *Phys. Rev. B* **1994**, *50*, 17953−17979.
(35) Ceperley, D. M.; Alder, B. J. Ground-State of the Electron-Gas by a Stochastic Method. *Phys. Rev. Lett.* **1980**, *45*, 566−569.

DOI: 10.1021/acsami.5b02782
ACS Appl. Mater. Interfaces 2015, 7, 12981−12987